Contemporary Engineering Sciences, Vol. 12, 2019, no. 2, 51 - 64
HIKARI Ltd, www.m-hikari.com
https://doi.org/10.12988/ces.2019.916

Thermo-Elastic Characteristics of Homogeneous Circular Disk Models Subjecting to a Contact Force

Jaegwi Go

Department of Applied Mathematics, Changwon National University
20 Changwondaehak-ro Uichang-gu, Changwon, Gyeongnam 641-773, Korea

Abstract

The thermo-elastic characteristics of a rotating *Al* homogeneous circular disk have been investigated by considering a contact force on a work piece area. A pair of partial differential equation is induced as a governing equations based on Hooke's law. Due to the complexity of the governing equations a finite volume model is applied to the problem to obtain approximate solutions. Contact force may not be ignorable parameter to determine thermo-elastic movements in rotating circular disk. Moreover, the numerical approximations yields that radial thickness is a crucial factor to control the thermo-elastic behavior of rotating circular disks.

Keywords: Circular disk, Contact force, Finite volume method, Thermo-elastic characteristics

1. Introduction

The thermo-elastic contact of a rotating circular disk induces complex processes such as friction, wear, heat generation, and temperature deformation. All parameters related with the behavior of a rotating circular disk are connected mutually and interactions are developed during the load of a contact force. Due to the complicated interactions the variation of each parameter yields deep effects to thermo-elastic movements. The investigation to the influences of temperature, contact pressure, and blushed wear in rotating circular disk still remains as a challenging work.

Circular disk is a practically useful shape in various industrial applications, and the physical movements of circular shaped models have been investigated by many researchers. The thermal stress behavior of a circular cylinder is analyzed by Obata and Noda, [1] and Liew *et al.* [2]. Kovalyshen [3] studied a circular disk cutter, and characterized that the movements of an oscillatory in operating process reduces cutting forces. Using Kirchhoff plate theory the radial component effects of the reaction force on the bending of thin circular plates are presented by Huang and Li [4]. Ren *et al*. [5] investigated the breakage of circular cutter ring during shield tunneling. They proved that the unbalance forces between two sides of cutter ring during cutting process are major reason for the cutting ring breakage. Weight function method is applied by Wu and Tong to determine stress intensity factors crack opening displacements in complicated stress fields for an edge-cracked circular disk [6].

Meanwhile, most of researches for the circular disks have been carried out without considering contact force during the cutting process, even though contact force is a crucial parameter in determination of the thermo-elastic characteristics [7-8]. Rad [9] investigated static behavior of the auxetic-porous structures composed of multi directional heterogeneous materials with considering friction force. The static response of non-uniform bi-directional functionally graded auxetic-porous material circular plates is carried out based on poroelasticity theory. Tadokoro *et al*. [10] applied the yaw angle misalignment theory to rotary contact systems for circular sliding contact. Parallel misalignment between drive and driven shafts stabilize the systems due to change in the direction of local frictional force. In the previous study [11], it has been demonstrated that by proper control some parameters such as temperature distribution, angular speed, and radial thickness improved thermos-elastic characteristics are obtained in the design of a circular or grinding disk.

The present study focuses on the analysis of thermo-elastic characteristics of a rotating Al homogeneous circular disk undergoing of a contact force. By considering of contact forces a pair of partial differential equations is derived using Hooke's law. A finite volume method is applied to the complicated governing equations to obtain the solution of displacement, stress, and stain components as a function of contact force and radial thickness.

2. Mathematical modeling

Rotating homogeneous circular disks with a concentric circular hole are taken into account (see Fig. 1). The origin of the polar coordinate system $r-\theta$ is assumed to be located at the center of the disk and hole. The radii of the hole and outer surface of the disk are designated by a and b, and the angular velocity, Young's modulus, CTE, the density of the disk are denoted by ω, E, α, and ρ, respectively. The angular velocity, denoted by ω, can be determined from the relation $\omega = 2\pi N/60$, $N$is the revolutions per minute (rpm).

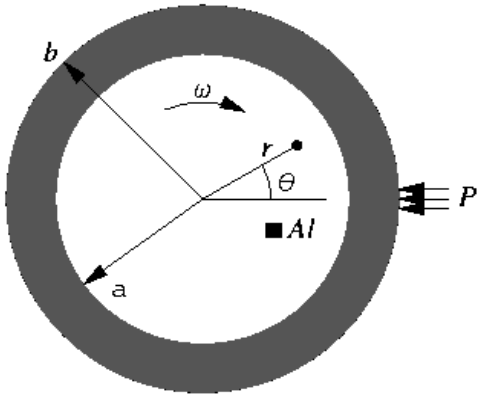

Figure 1.Schematic diagram of homogeneous circular disk model

2.1. Temperature distribution profiles

Based on the assumption that the disk is subjecting to the loading of symmetric temperature to the radial direction, the differential equation expressing the temperature distribution profile in the polar coordinates

$$\frac{1}{r}\frac{\partial}{\partial r}\left(r\frac{\partial T}{\partial r}\right)=0. \tag{1}$$

The general solution of equation (1) is of the form

$$T(r)=c_1 \ln r + c_2, \tag{2}$$

where c_1 and c_2 are integral constants and will be determined on account of the boundary conditions.

2.2. Thermoelastic characteristics

Let u and v be the components of the displacement of a deformed circular disk to the radial and circumferential directions, and let ε_r and ε_θ be the strains to the radial and circumferential directions, respectively, and γ denotes shearing strains. Then, strain components are expressed in terms of deformation components as follows:

$$\varepsilon_r=\frac{\partial u}{\partial r}\ \varepsilon_\theta=\frac{1}{r}\frac{\partial v}{\partial \theta}+\frac{u}{r}\ \varepsilon_z=0$$
$$\gamma_{r\theta}=\frac{1}{r}\frac{\partial u}{\partial \theta}+\frac{\partial v}{\partial r}-\frac{v}{r}\ \gamma_{z\theta}=0\ \gamma_{rz}=0 \tag{3}$$

Let σ_r and σ_θ be the radial and circumferential stress components, respectively, and τ implies shearing stress. From the Hooke's law in plane stress problems, the strain-stress relations undergoing thermal expansion, in polar coordinates, are written by

$$\varepsilon_r=\frac{1}{E}[\sigma_r-\upsilon\sigma_\theta]+\alpha T\ \ \varepsilon_\theta=\frac{1}{E}[\sigma_\theta-\upsilon\sigma_r]+\alpha T$$

$$\tau_{r\theta} = \frac{E}{2(1+\nu)}\gamma_{r\theta}\ \tau_{\theta z} = 0\ \tau_{rz} = 0 \tag{4}$$

Here, $T(r)$ is the change in temperature at any distance r and ν denotes Poisson's ratio. Note that equilibrium equations in polar coordinates are as follows:

$$\frac{\partial \sigma_r}{\partial r} + \frac{1}{r}\frac{\partial \tau_{r\theta}}{\partial \theta} + \frac{\sigma_r - \sigma_\theta}{r} + \rho\omega^2 r = 0$$
$$\frac{\partial \sigma_\theta}{\partial \theta} + r\frac{\partial \tau_{r\theta}}{\partial r} + 2\tau_{r\theta} = 0 \ . \tag{5}$$

The combination of equations (3)– (5) leads to the following governing equations:

$$\frac{\partial}{\partial r}(r\frac{\partial u}{\partial r}) + \frac{1-\upsilon}{2r}\frac{\partial^2 u}{\partial \theta^2} - \frac{3-\upsilon}{2r}\frac{\partial v}{\partial \theta} + \frac{1+\upsilon}{2}\frac{\partial^2 v}{\partial r \partial \theta} - \frac{u}{r} + \frac{1-\upsilon^2}{E}\rho\omega^2 r^2 = (\upsilon+1)\alpha r\frac{dT(r)}{dr}$$
$$\frac{1-\upsilon}{2}\frac{\partial}{\partial r}(r\frac{\partial v}{\partial r}) + \frac{1}{r}\frac{\partial^2 v}{\partial \theta^2} + \frac{3-\upsilon}{2r}\frac{\partial u}{\partial \theta} + \frac{1+\upsilon}{2}\frac{\partial^2 u}{\partial r \partial \theta} - \frac{1-\upsilon}{2}\frac{v}{r} = 0 \tag{6}$$

For the present rotating homogeneous disk subjecting to contact forces the following boundary conditions

$$\sigma_r(a,\theta) = 0\,, \quad \sigma_r(b, \theta - \{0\}) = 0\,, \quad \sigma_r(b,0) = P \ \text{ at contact point}$$

are applied.

2.3 Finite volume formulation.

A pair of the governing equations is too involved to be solved analytically. A numerical technique thus is required for the approximation and a finite volume method is applied. The domain is divided up into control volume and integrates the field equations over each control volume (see Fig. 2). The finite surface mesh is denoted by (i, j) and the discretizations for the governing equations are developed based on the following relations at the adjacent locations;

$$(\frac{\partial u}{\partial r})_{i,j+\frac{1}{2}} = \frac{u_{i,j+1} - u_{i,j}}{\Delta r}, \qquad (\frac{\partial u}{\partial r})_{i,j-\frac{1}{2}} = \frac{u_{i,j} - u_{i,j-1}}{\Delta r}, \qquad (\frac{\partial u}{\partial r})_{i,j-1} = \frac{u_{i,j+1} - u_{i,j-1}}{2\Delta r}$$
$$(\frac{\partial w}{\partial z})_{i,j} = \frac{1}{2\Delta z}(3w_{i,j} - 4w_{i-1,j} + w_{i-2,j})$$
$$w_{m+\frac{1}{2},j+1} = w_{m,j+1} + \frac{1}{4}(3w_{m,j+1} - 4w_{m-1,j+1} + w_{m-2,j+1})$$
$$w_{m-\frac{1}{2},j+1} = w_{m-1,j+1} + \frac{1}{4}(w_{m,j+1} - w_{m-2,j+1})$$

$$\phi_{i+\frac{1}{2},\,j+\frac{1}{2}} = \frac{1}{2}\left(\phi_{i+\frac{1}{2},\,j+1} + \phi_{i+\frac{1}{2},\,j}\right). \tag{7}$$

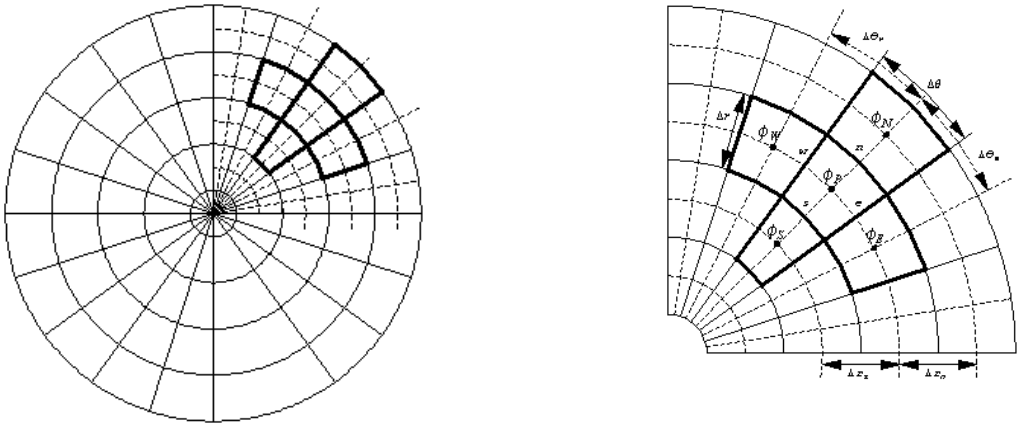

(a) (b)

Figure 2. (a) Discretization of circular disk domain, (b) Notations of finite control volumes

The subscript $\frac{1}{2}$ implies the value of the displacement at the boundary of the control surface (see Fig. 2(b)). According to above relations at the adjacent locations the equations (6) are discretized as below:

$$A_{11}u_{i+1,\,j} + A_{12}u_{i,\,j+1} + A_{13}u_{i,\,j} + A_{14}u_{i,\,j-1} + A_{15}u_{i-1,\,j}$$
$$+ B_{11}v_{i,\,j+1} + B_{12}v_{i,\,j} + B_{13}v_{i,\,j-1} + B_{14}v_{i-1,\,j+1} + B_{15}v_{i-1,\,j} + B_{16}v_{i-1,\,j-1} + B_{17}v_{i-2,\,j+1} + B_{18}v_{i-2,\,j} + B_{19}v_{i-2,\,j-1} = f_{i,\,j}$$

$$A_{21}u_{i,\,j+1} + A_{22}u_{i,\,j} + A_{23}u_{i,\,j-1} + A_{24}u_{i-1,\,j+1} + A_{25}u_{i-1,\,j} + A_{26}u_{i-1,\,j-1} + A_{27}u_{i-2,\,j+1} + A_{28}u_{i-2,\,j} + A_{29}u_{i-2,\,j-1}$$
$$+ B_{21}v_{i+1,\,j} + B_{22}v_{i,\,j+1} + B_{23}v_{i,\,j} + B_{24}v_{i,\,j-1} + B_{25}v_{i-1,\,j} = 0$$

$$A_{11} = \frac{1-\upsilon}{2}\frac{\Delta r}{\Delta\theta}\frac{1}{r_{i,\,j}},\quad A_{12} = \frac{\Delta\theta}{\Delta r}r_{i,\,j+\frac{1}{2}},\quad A_{13} = -\frac{\Delta\theta}{\Delta r}\left(r_{i,\,j+\frac{1}{2}} + r_{i,\,j-\frac{1}{2}}\right) - (1-\upsilon)\frac{\Delta r}{\Delta\theta}\frac{1}{r_{i,\,j}} - \Delta r\Delta\theta\frac{1}{r_{i,\,j}},$$

$$A_{14} = \frac{\Delta\theta}{\Delta r}r_{i,\,j-\frac{1}{2}},\qquad A_{15} = \frac{1-\upsilon}{2}\frac{\Delta r}{\Delta\theta}\frac{1}{r_{i,\,j}},\quad B_{11} = \frac{3}{8}(1+\upsilon),\qquad B_{12} = -\frac{3}{4}(3-\upsilon)\Delta r\frac{1}{r_{i,\,j}},$$

$$B_{13} = -\frac{7}{16}(1+\upsilon),\quad B_{14} = -\frac{1}{2}(1+\upsilon),\qquad B_{15} = \frac{5}{2}(3-\upsilon)\frac{1}{r_{i,\,j}},\quad B_{16} = \frac{9}{16}(1+\upsilon),$$

$$B_{17} = \frac{1}{8}(1+\upsilon),\qquad B_{18} = -\frac{3}{4}(3-\upsilon)\Delta r\frac{1}{r_{i,\,j}},\quad B_{19} = -\frac{1}{8}(1+\upsilon),$$

$$f_{i,j} = (1+\upsilon)\alpha r_{i,j}\Delta\theta(T_{i,j+\frac{1}{2}} - T_{i,j-\frac{1}{2}}) - \Delta r\Delta\theta\rho\omega^2 \frac{1-\upsilon^2}{E} r_{i,j}^2,$$

$$A_{21} = \frac{3}{8}(1+\upsilon), \quad A_{22} = \frac{3}{4}(3-\upsilon)\Delta r\frac{1}{r_{i,j}}, \quad A_{23} = -\frac{7}{16}(1+\upsilon), \quad A_{24} = -\frac{1}{2}(1+\upsilon),$$

$$A_{25} = -(3-\upsilon)\Delta r\frac{1}{r_{i,j}}, \quad A_{26} = \frac{9}{16}(1+\upsilon), \quad A_{27} = \frac{1}{8}(1+\upsilon), \quad A_{28} = (3-\upsilon)\Delta r\frac{1}{r_{i,j}},$$

$$A_{29} = -\frac{1}{8}(1+\upsilon), B_{21} = \frac{\Delta r}{\Delta\theta}\frac{1}{r_{i,j}}, B_{22} = \frac{\Delta\theta}{\Delta r} r_{i,j+\frac{1}{2}}$$

$$B_{23} = -\frac{\Delta\theta}{\Delta r}(r_{i,j+\frac{1}{2}} + r_{i,j-\frac{1}{2}}) - \frac{1-\upsilon}{2}\Delta r\Delta\theta\frac{1}{r_{i,j}} - 2\frac{\Delta r}{\Delta\theta}\frac{1}{r_{i,j}}, \quad B_{24} = \frac{\Delta\theta}{\Delta r} r_{i,j-\frac{1}{2}}, \quad B_{25} = \frac{\Delta r}{\Delta\theta}\frac{1}{r_{i,j}}.$$

3. Numerical results and discussion

In this section, the finite volume formula developed in section 2.3 applied to obtain numerical results of different components of displacement, stress, and strain for a *Al* homogeneous circular disk. The temperature distribution profile and thermo-elastic characteristics are evaluated based on the mechanical and thermal properties shown in Table 1.

Material/Property	Elastic module (MPa)	Thermal expansion coefficient (10^{-6}/°C)	Thermal conductivity (W/m-°C)	Density (g/cm^3)
Al	71	23.1	237	2.70

Table 1. Mechanical and thermal properties used in this study for analyzing thermoelastic characteristics.

Fig. 3 displays the temperature distribution profiles, which is obtained according to the process in the section 2.1. T_a and T_b imply temperature degree of inner and outer boundaries , respectively, to determine the integral constants for the temperature distribution profiles. The temperature distribution increases logarithmically as radius$r$ increases.

The displacement distributions are presented in Fig. 4. Fig. 4(a) shows displacement to the radial direction at the representative angles: $\theta = 90$, $\theta = 180$, and $\theta = 270$. The largest radial displacement occurs at $\theta = 0$, and the magnitude decreases as angle value θ increases. The magnitude of radial displacement varies dramatically near outer boundary area. The circumferential displacement distributions are exhibited in Fig. 4(b) at the representative normalized values $r-a/b-a=$ 0.1, 0.5, and 0.9. The circumferential displacement fluctuates near the contact point ($r-a/b-a=0.9$), while the circumferential displacement develops to the center of the circular disk around the inner boundary ($r-a/b-a=0.1$). Middle area ($r-a/b-a=0.5$) of the circular disk is undergoing trivial influence in the circumferential displacement distribution.

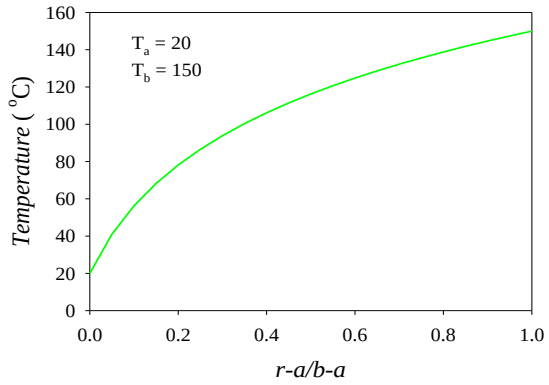

Figure 3.Temperature distribution along the radial direction

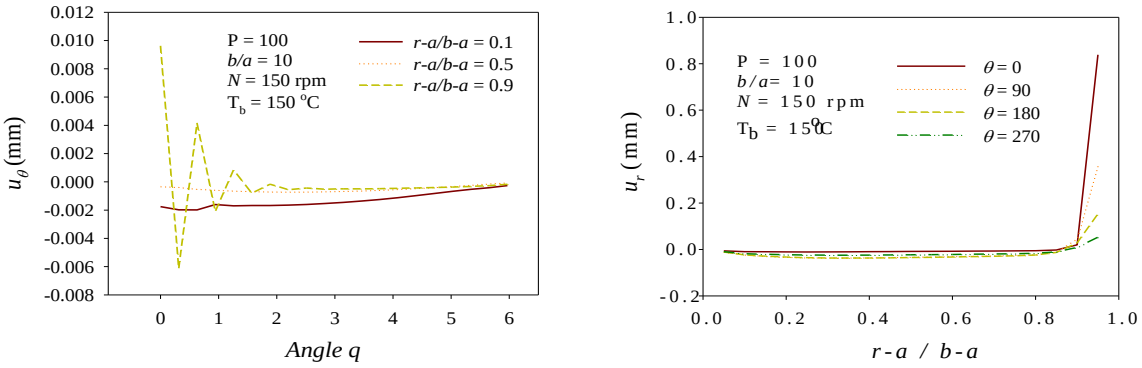

(a) (b)

Figure 4. Displacement distribution profiles: (a)radial, (b) circumferential

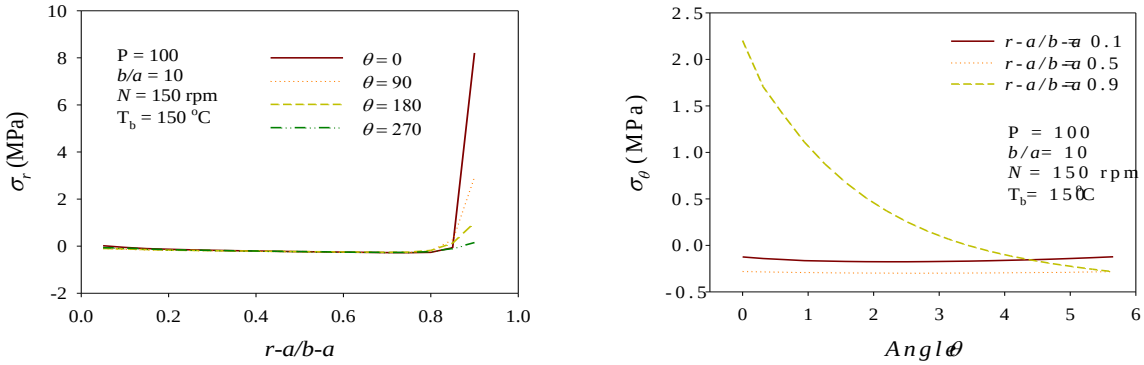

(a) (b)

Figure 5. Stress distribution profiles: (a) radial, (b) circumferential

Fig. 5 displays stress distribution profiles. The radial stress distributions are prescribed along the radial direction in Fig. 5(a). Most of disk area is influenced by tensile radial stress, and the largest radial stress occurs at the contact point. The magnitude of radial stress is getting smaller as the angle value is getting larger. Meanwhile, compressive circumferential stress appears at normalized values $r-a\,/\,b-a=0.1$ and 0.5. But, most area experiences tensile stress at $r-a\,/\,b-a=0.9$ (see fig. 5(b)). Fig. 6 displays strain distribution profiles. As shown in Fig. 6(a), positive radial strain distribution appears and the magnitude

of radial strain increases with the increase of angle value. The contact point generates the largest radial strain value. Different tendency develops in the circumferential strain distribution. While the circumferential strain value is negative at $r-a\,/\,b-a=0.1$ and 0.5, positive circumferential strain is exposed for the value $r-a\,/\,b-a=0.9$ (see Fig. 6(b)). The largest magnitude comes out around $\theta=0.2$ with $r-a\,/\,b-a=0.9$.

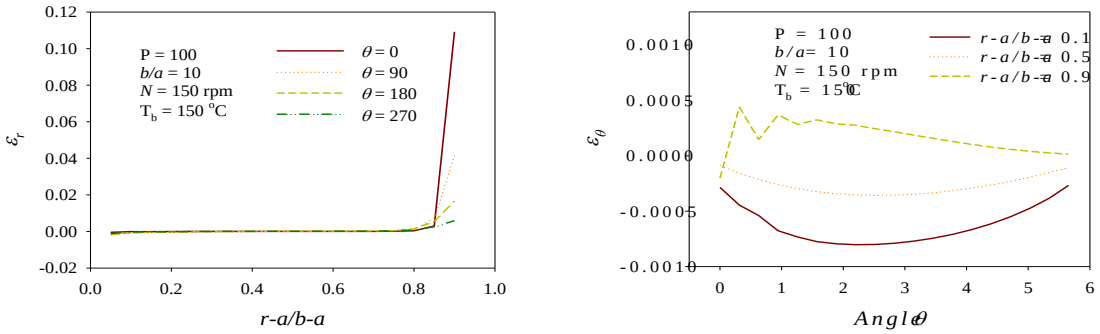

(a) (b)

Figure 6. Strain distribution profiles: (a) radial, (b) circumferential

The effects of contact force to the thermo-elastic characteristics are expressed through Fig. 7 to 9. The representative contact force 100, 300, 500, and 700 are applied. Fig. 7 describes the influence of contact force to the displacement distribution. As shown in Fig. 7(a) and 7(b), the magnitude of radial displacement is getting larger as the contact force increases near the outer boundary of circular disk. The effects of contact force to circumferential displacement is trivial near the inner boundary of circular disk (see Fig. 7(c)), whereas the variation for contact force yields significant influence near the outer boundary of circular disk (see Fig. 7(d)). As the contact force is getting larger, greater magnitude shows up.

The influences of contact force for the stress distribution are described in Fig. 8. Both angle values ($\theta=0$ and 180) are under the deep impact to the change of contact force in radial stress distribution and the magnitude increases with increase of contact force (see Fig. 8(a) and (b)). While trivial effect exhibits in circumferential stress near the inner boundary of the circular disk (see Fig. 8(c)), outer boundary of circular disk reacts sensitively to the change of contact force. The largest influence arises with the variation of contact force when $\theta=0$ (see Fig. 8(d)). Fig. 9 exhibits the effects of contact force to the strain distributions. By the increase of contact force at $\theta=0$ nearby area of outer boundary is excessively susceptible, and the radial strain distributions upsurges to the positive direction (see Fig. 9(a)). But, as shown in Fig. 9(b), different phases develop at $\theta=180$. The radial strain distribution is increasing to the positive direction until around the value $r-a\,/\,b-a=0.9$, and is decreasing as the value $r-a\,/\,b-a$ approaches to outer boundary. The influence of contact force around inner circular disk boundary is trivial to the circumferential strain, while nearby area of outer boundary displays sensitive reactions to the change of contact force (see Fig. 9(c) and 9(d)). Remarkable alteration in the circumferential strain distribution occurs close by $\theta=0$.

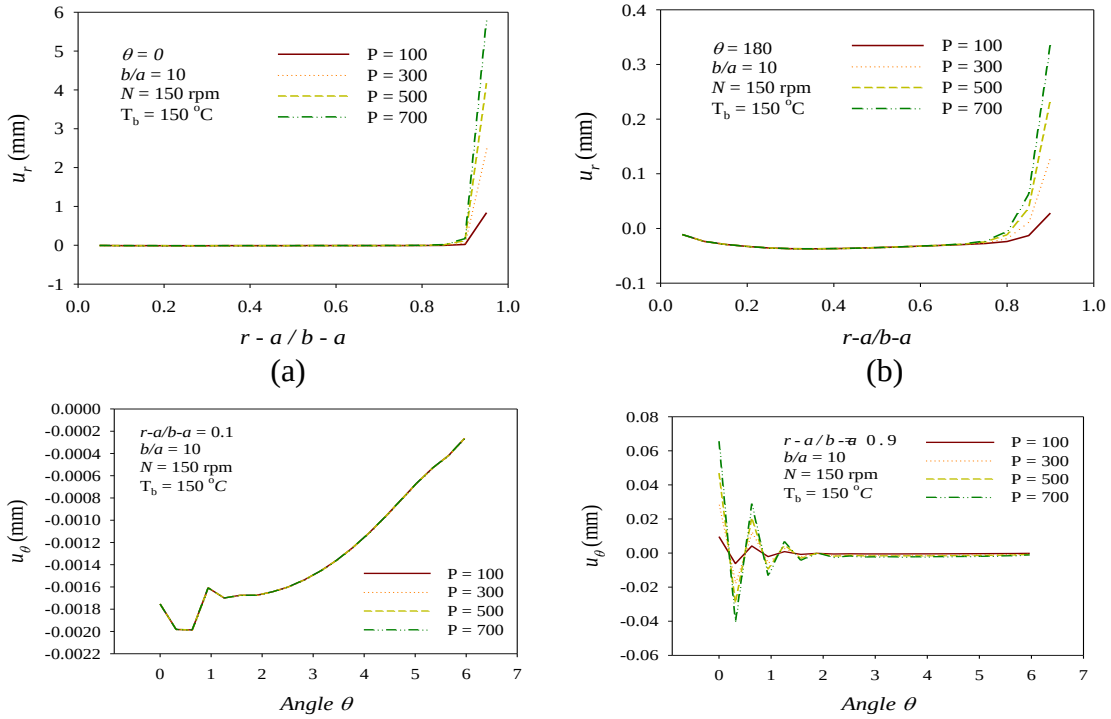

Figure 7. Effects of contact force on the component of displacement: (a) radial $\theta = 0$, (b) radial $\theta = 180$, (c) circumferential $r - a / b - a = 0.1$, (d) circumferential $r - a / b - a = 0.9$

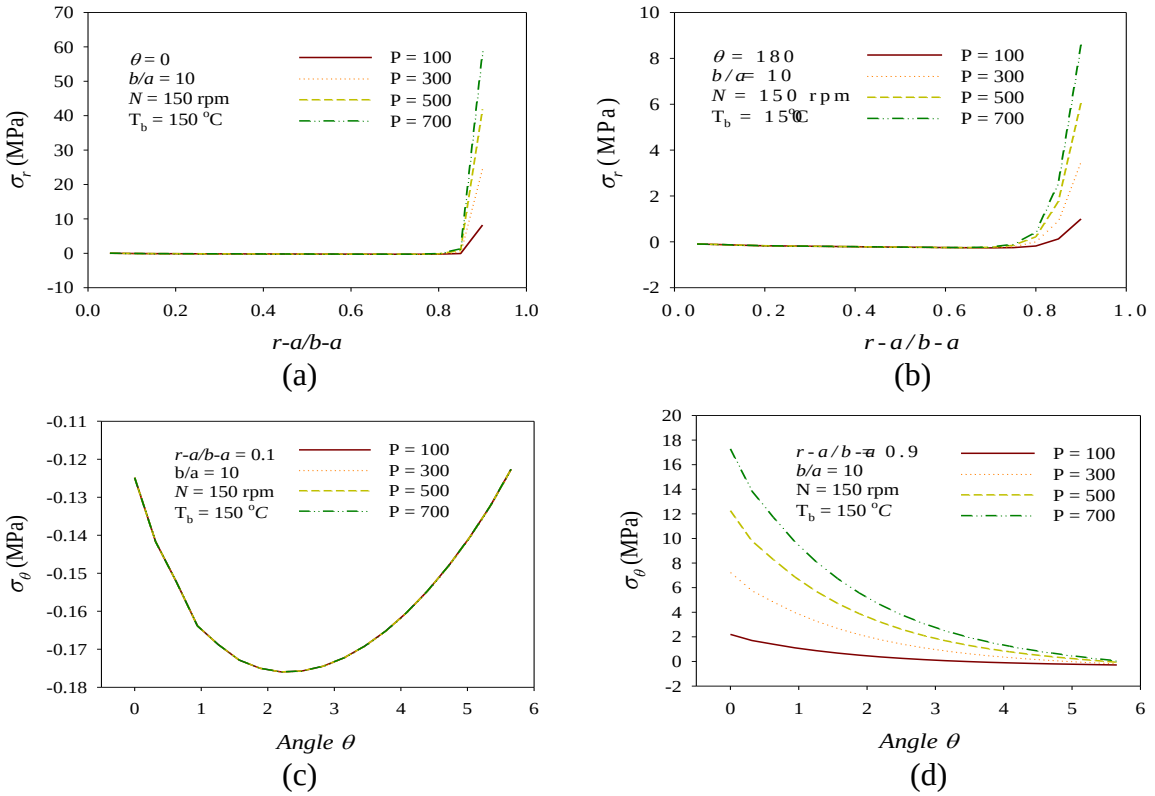

Figure 8. Effects of contact force on the component of stress: (a) radial $\theta = 0$, (b) radial $\theta = 180$, (c) circumferential $r - a / b - a = 0.1$, (d) circumferential $r - a / b - a = 0.9$

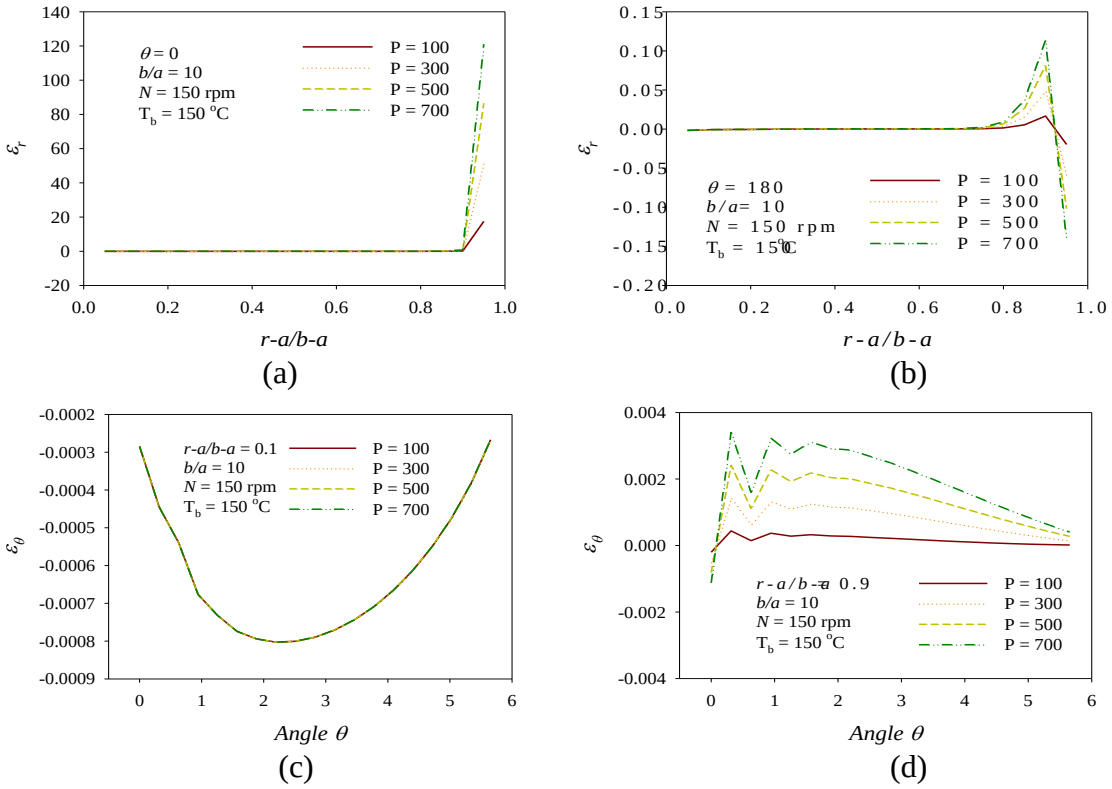

Figure. 9. Effects of contact force on the component of strain: (a) radial $\theta = 0$, (b) radial $\theta = 180$, (c) circumferential $r-a\,/\,b-a$ = 0.1, (d) circumferential $r-a\,/\,b-a$ = 0.9

The influences of the b/a values to thermo-elastic characteristics are explained through Fig. 10 to 12. The value of the ratio b/a implies the measure of the radial thickness of the circular disk. The representative values b/a =5, 10, and 20 are chosen. The effects in the radial displacement distribution are appeared in Fig. 10(a) and 10(b) according to the change of b/a. The magnitude of the radial displacement distribution decreases as the value b/a increases, and the influences by the variation of b/a weakens with increase of $r-a\,/\,b-a$. The circumferential displacement distributions expose different phases, as shown in Fig. 10(c). The magnitude of circumferential displacement is getting larger as the value $r-a\,/\,b-a$ is growing at $r-a\,/\,b-a$ = 0.1. The effect due to b/a is trivial at $r-a\,/\,b-a$ = 0.9 except inner area of circular disk (see Fig. 10(d)). By the variation of the b/a values the radial stress distributions are expressed in Fig. 11(a) and 11(b). As the value b/a increases larger compressive radial stress develops up to around $r-a\,/\,b-a$ = 0.8, and smaller tensile radial stress is appeared after around $r-a\,/\,b-a$ = 0.8. The results imply that the larger b/a value yields more stable structure in grinder manufacture. Similar movements come out in circumferential stress distributions. With the increase of b/a, larger compressive circumferential stress is exhibited nearby area of inner boundary (see Fig. 11(c)), while smaller tensile circumferential stress turns up around outer boundary of circular disk (see Fig. 11(d)).

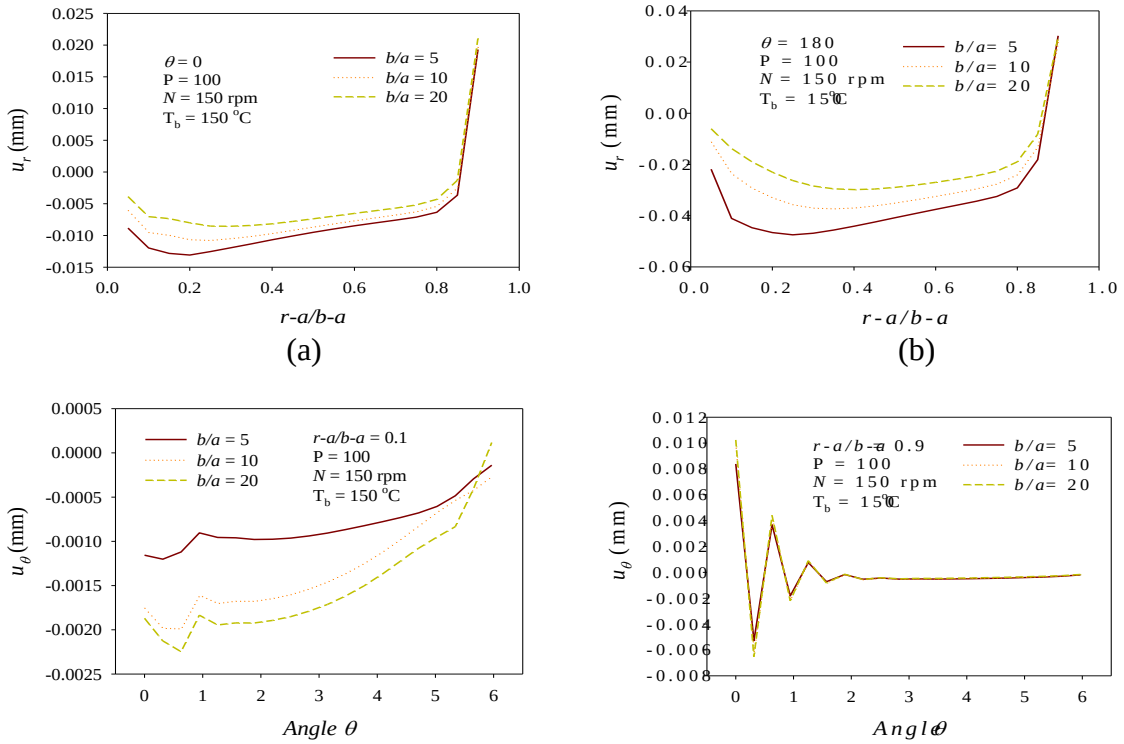

Figure 10. Effects of radial thickness on the component of displacement: (a) radial $\theta = 0$, (b) radial $\theta = 180$, (c) circumferential $r - a / b - a = 0.1$, (d) circumferential $r - a / b - a = 0.9$

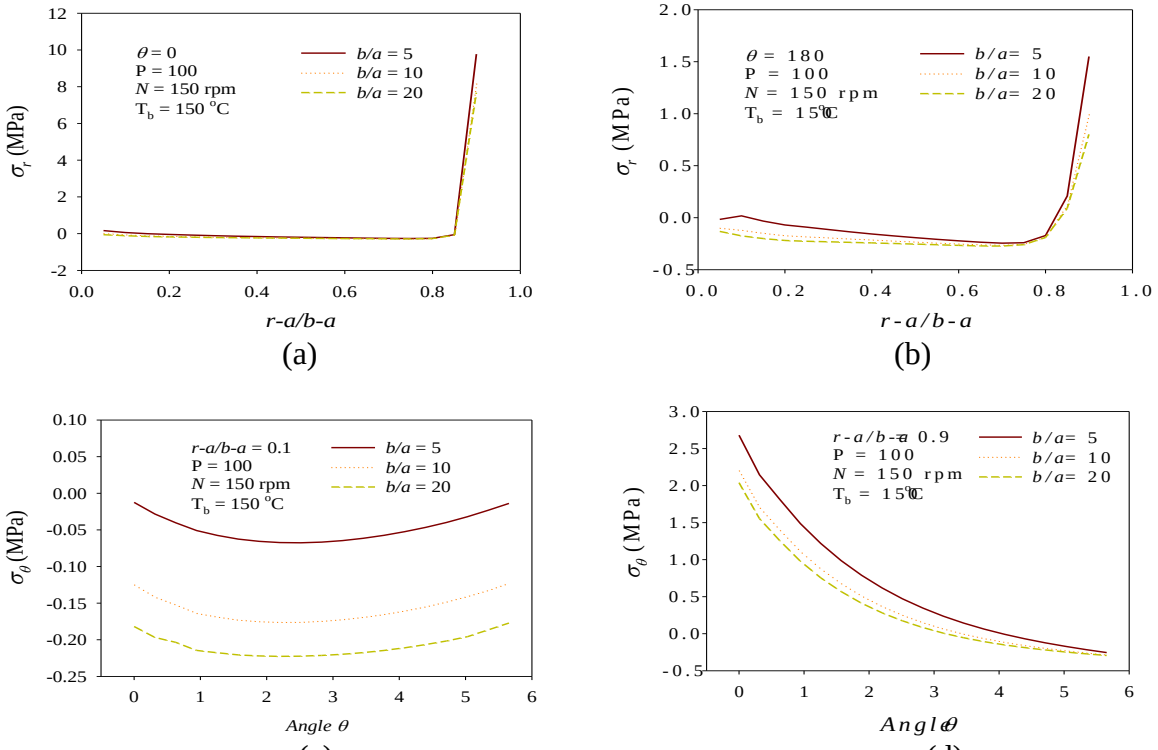

Figure 11. Effects of radial thickness on the component of stress: (a) radial $\theta = 0$, (b) radial $\theta = 180$, (c) circumferential $r - a / b - a = 0.1$, (d) circumferential $r - a / b - a = 0.9$.

The effects of b/a to the strain distribution are presented in Fig. 12. As shown in Fig. 12(a) and 12(b), the radial strain sits loose to the variation of the value b/a except near area of circular boundaries. At the both boundaries the radial strain magnitude is getting smaller with increase of the value b/a. Around nearby area of inner boundary the magnitude of circumferential strain decreases with increase of b/a (see Fig. 12(c)), whereas the circumferential strain displays larger behavior according to the increase of b/a around outer boundary of circular disk (see Fig. 12(d)).

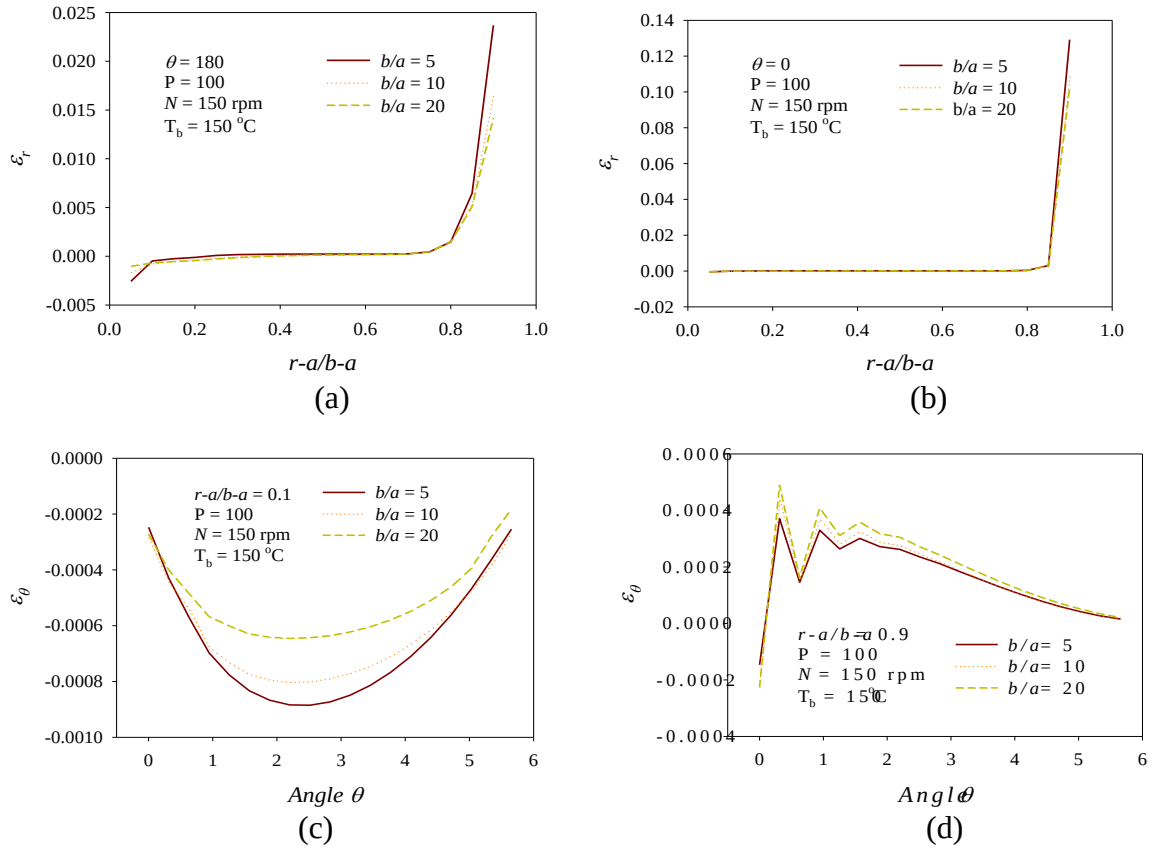

Figure 12. Effects of radial thickness on the component of strain: (a) radial $\theta = 0$, (b) radial $\theta = 180$, (c) circumferential $r - a / b - a$ = 0.1, (d) circumferential $r - a / b - a$ = 0.9

4. Conclusions

The thermo-elastic characteristics of homogeneous circular disks undergoing contact forces have been investigated using a finite volume method. By the variation of contact force and radial thickness the influences to the components of displacement, stress, and strain have been presented. It is found that the thermo-elastic characteristics of *Al* homogeneous circular disks are deeply depend on the contact forces and radial thickness, and the behavior can be controlled by controlling of these parameters. Therefore, the finite volume analysis used in this investigation can be applied on the design of an *Al* homogeneous circular cutter or grinding disk subjecting to a loading pressure to promote proper and reliable thermo-elastic characteristics in service.

Acknowledgements. This research was supported by Basic Science Research Program through the National Research Foundation of Korea (NRF) funded by the Ministry of Education (2018-0182).

References

[1] Y. Obata and N. Noda, Steady thermal stress in a hollow circular cylinder and a hollow sphere of a functionally gradient materials, *J. Therm. Stress*, **17** (1994), 471-487. https://doi.org/10.1080/01495739408946273

[2] K.M. Liew, S. Kitipornchai, X.Z. Zhang, and C.W. Lim, Analysis of the thermal stress behavior of functionally graded hollow circular cylinders, *Int. J. Solids Struct*., **40** (2003), 2355-2380. https://doi.org/10.1016/s0020-7683(03)00061-1

[3] Y. Kovalyshen, Analytical model of oscillatory disc cutting, *Int. J. Rock Mechanics & Mining Sciences*, **77** (2015), 378-383. https://doi.org/10.1016/j.ijrmms.2015.04.015

[4]. Y. Huang and X.-F. Li, Effect of radial reaction force on the bending of circular plates resting on a ring support, *Int. J. Mechanical Sciences*, **119** (2016), 197-207. https://doi.org/10.1016/j.ijmecsci.2016.10.014

[5] D.-J. Ren, J.S. Shen, J.-C. Chai, and A. Zhou, Analysis of disc cutter failure in shield tunneling using 3D circular cutting theory, *Engineering Failure Analysis*, **90** (2018), 23-35. https://doi.org/10.1016/j.engfailanal.2018.02.015

[6] X.R. Wu and D.H. Tong, Evaluation of various analytical weight function methods base on exact K-solutions of an edge-cracked circular disc, *Engineering Fracture Mechanics*, **189** (2018), 64-80. https://doi.org/10.1016/j.engfracmech.2017.09.024

[7] T. Dai and H.-L. Dai, Analysis of a rotating FGMEE circular disk with variable thickness under thermal environment, *Applied Mathematical Modelling*, **45** (2017), 900-924. https://doi.org/10.1016/j.apm.2017.01.007

[8] H.-L. Dai, Z.-Q. Zheng, and T. Dai, Investigation on a rotating FGPM circular disk under a coupled hygrothermal field, *Applied Mathematical Modelling*, **46** (2017), 28-47. https://doi.org/10.1016/j.apm.2017.01.062

[9] A.B. Rad, Static analysis of non-uniform 2D functionally graded auxetic-porous circular plates interacting with the gradient elastic foundations involving friction force, Aerospace Science and Technology, 76 (2018), 315-339. https://doi.org/10.1016/j.ast.2018.01.036

[10] C. Tadokoro, T. Nagamine, and K. Nakano, Stabilizing effect arising from parallel misalignment in circular sliding contact, *Tribology International*, **120** (2018), 16-22. https://doi.org/10.1016/j.triboint.2017.12.003

[11] J. Go, A.M. Afsar, and J. Song, Analysis of thermoelastic characteritics of a rotating FGM circular disk by finite element method, *Adv. Compos. Mater.*, **19** (2010), 197-213. https://doi.org/10.1163/092430410x490473

Received: February 1, 2019; Published: March 14, 2019